



Experimental study of the instabilities of alongshore currents on plane beaches

Chunping Ren^{a,b,*}, Zhili Zou^b, Dahong Qiu^b

^a College of Water Resource Science and Engineering, Taiyuan University of Technology, Taiyuan 030024, China

^b The State Key Laboratory of Coastal and Offshore Engineering, Dalian University of Technology, Dalian 116024, China

ARTICLE INFO

Article history:

Received 4 October 2010

Received in revised form 8 July 2011

Accepted 19 July 2011

Available online 19 August 2011

Keywords:

Breaking waves

Alongshore currents

Shear instability

Linear instability analysis

ABSTRACT

A laboratory experiment on alongshore currents was conducted for two plane beaches, with gradients 1:40 and 1:100, to investigate the instability of alongshore currents. Complicated and strongly unstable alongshore current motions were observed. In order to clearly examine the spatial and temporal variations of the shear instability of the currents, digital images from a charge-coupled device (CCD) recorded the deformations of dye batches released in the surf zone. Some essential characteristics of the shear instability were obtained from analyses of images showing the temporal variation of the dye patches.

A high-resolution spectral analysis technique (the maximum entropy method, or MEM) was used to analyze the dominant frequency of the observed oscillation, along with the trigonometric regression method for determining the variations of the oscillation strength in the cross-shore direction. The propagation speed of the dye patch was obtained by tracking the movement over time of fixed locations in the dye patch, such as its peak, in the longshore direction. This data was then fitted linearly.

Alongshore and cross-shore velocity time series acquired from sensors showed clearly that large-amplitude, long-period (about 50 s or 100 s) oscillations were present for all sensors deployed in the cross-shore direction under regular and irregular wave conditions. The analysis found that the maximum shear wave amplitude was approximately one-sixth of the maximum for the mean alongshore current, and occurred approximately at the position of the maximum of the mean alongshore current for irregular waves. The spatial structure of the shear waves was studied by analyzing collected images of the dye patches. The phase velocity of the meandering movements was obtained by measuring the magnitude of the oscillations of the dye patches in the alongshore direction with respect to time. The results suggest that the propagation speed of the shear instability was approximately one-half to three-quarters of the maximum mean longshore current for both regular and irregular waves.

Linear instability analysis theory was applied to the characteristics of alongshore current instability, which suggested that there are two instability modes related to the observed oscillations: the frontshear mode observed for the 1:100 slope, and the backshear mode observed for the 1:40 slope. Theoretical analyses agreed with the experimental results in both cases. The velocity profile of the mean longshore current was found to affect the instability mode significantly, leading to further investigations on the influence of the velocity profiles and to provide support for the above conclusions.

© 2011 Elsevier B.V. All rights reserved.

1. Introduction

Field experiments of longshore currents on a sandy beach near Duck, North Carolina were conducted by Oltman-Shay et al. (1989) who identified oscillations associated with the presence of alongshore currents. These oscillations were too short in magnitude to be surface waves due to gravity at the observed frequencies, and had longer periods (1000 s) than gravity waves. Bowen and Holman (1989) first described the essential dynamic of this instability and illustrated the

mechanism of shear instability in terms of background vorticity. Such oscillations are called shear waves. Subsequent field experiments performed by Noyes et al. (2004) showed that the total root mean square shear wave fluctuations are between 10% and 40% of the locally observed mean alongshore current, and shear waves are generated primarily in the highly sheared region immediately seaward of the location of the maximum mean alongshore current velocity V_{\max} . The observed cross-shore and alongshore structures of shear waves are similar to the linearly unstable modes predicted by linear instability theory.

Laboratory experiments on the shear instability of longshore currents have been carried out, for instance by Visser et al. (1982) who experimented on alongshore currents on plane slopes 1:10 and 1:20, but their experimental results did not indicate the temporal variations of alongshore currents. Measurements of the unstable

* Corresponding author at: College of Water Resource Science and Engineering, Taiyuan University of Technology, Taiyuan 030024, China. Tel.: +86 351 6010102; fax: +86 351 6010102.

E-mail address: chunpingren@163.com (C. Ren).

motion of alongshore currents by Reniers et al. (1997) suggested that instability occurs on a barred beach but not on a non-barred beach; however, although they observed oscillations for both regular waves and random waves on a barred beach, Reniers et al. (1997) suggested that such observations do not necessarily preclude shear instability on a plane beach. Putrevu and Svendsen (1992) attributed the lack of detection of shear waves in laboratory experiments to the limited length of the wave basin and the damping effect of bottom friction (the viscous damping probably suppressing the shear instability in laboratory experiments).

The present study examined whether shear instability does occur – and, if so, how it behaves on a plane slope – by performing a laboratory simulation of longshore currents on differently sloping plane beaches under different wave conditions (regular and irregular waves). A particular study was carried out as to whether the assumption that the eigenvalue with the largest imaginary component dominates the instability of that wavenumber was valid for all cases in the present experiment, bearing in mind that many previous researchers have employed the assumption when investigating shear instabilities since it was first proposed by Bowen et al. (1989). Tiessen et al. (2010) developed an algorithm to identify the more physically significant model predictions, but their predictions were still based on this assumption. The present study is significant in gaining an understanding of the physics of the formation of such rhythmic crescent-shaped

features, and is particularly useful for coastal engineers when making quantitative predictions in the field.

Waves incident on a beach induce different alongshore currents depending on whether they are regular waves produced by sea swell or random waves produced by wind. The shear instability of longshore currents occurs as a result of these flows. For similar incident wave heights, the longshore current velocity profile is narrow for regular waves due to the temporally constant wave height, but a broader velocity profile results from the temporal and spatial variation of the height of random waves. The influence of the different incident wave types and velocity profiles on the instability characteristics of the longshore currents were investigated in the present study. Previously, researchers have not paid particular attention to this problem. Haller and Kirby (1999) did a numerical study on the effects of lateral mixing and friction coefficient on the mean longshore current and the corresponding shear wave (the shear instability of longshore currents). They suggested that decrease in friction coefficient leads to a stronger mean longshore current and a faster, more energetic vortex structure produced by the shear instability of longshore current, and that an increase in the mixing coefficient causes relatively small variations in the propagation speeds of the shear waves.

Variations in longshore current velocity gradients in the surf zone cause the shear instability to increase, according to the linear

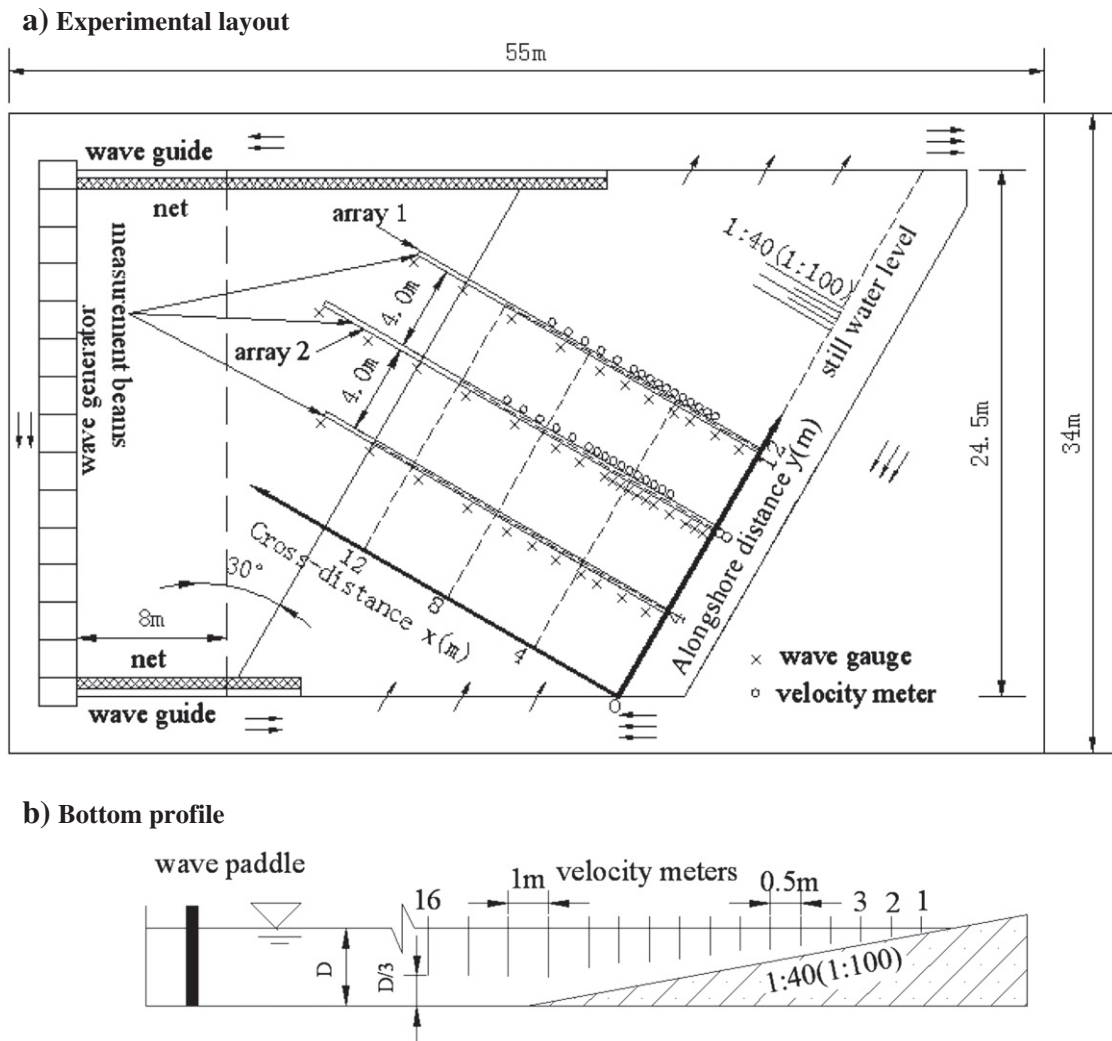


Fig. 1. Experimental set-up.

Table 1
The distances (x) of velocity meters from the shoreline.

VM	x (m)		VM	x (m)	
	Slope (1:40)	Slope (1:100)		Slope (1:40)	Slope (1:100)
1	1.5	2.0	9	5.5	6.0
2	2.0	2.5	10	6.0	6.5
3	2.5	3.0	11	6.5	7.0
4	3.0	3.5	12	7.0	8.0
5	3.5	4.0	13	8.0	9.0
6	4.0	4.5	14	9.0	10.0
7	4.5	5.0	15	10.0	11.0
8	5.0	5.5	16	11.0	12.0

instability theory of Bowen and Holman (1989). Shear waves are observed when the driving velocity gradients are energetic. The velocity gradient profile of alongshore currents for irregular waves is stronger than for regular waves of similar height. Therefore, although it can be speculated that shear waves are more likely to be observed when the waves are irregular, this does not imply that shear waves do not also occur in the case of regular waves. The present experimental results show that shear waves occur for both regular and irregular waves of large amplitude.

Baquerizo et al. (2001) proved the existence of instability due to the presence of a second extremum of background vorticity at the front side of longshore currents. The frontshear and backshear waves may have similar growth rates, with similar wave number and angular frequency, leading to the possibility of modulated shear waves. Their results from a case study on a planar beach showed that increased shear on the shoreward side of the mean current was required for unstable modes to appear due to the background vorticity (the cross-shore gradient of the longshore current velocity) at the shoreward side of the longshore current velocity profile. The existence of another instability mode, the backshear mode, has been recognized in many

studies (Bowen and Holman, 1989; Dodd and Thornton, 1990; Noyes et al., 2004; Putrevu and Svendsen, 1992) as being due to the extremum of the cross-shore gradient of the longshore current velocity at the seaward side of the longshore current velocity profile. This suggests that the shear instability of longshore currents is sensitive to the configuration of the background velocity profile. The present study gives a more detailed analysis of this problem by examining the longshore current instability on 1:100 and 1:40 slopes, and shows that the former is dominated by the frontshear instability mode and the latter by the backshear instability mode.

This paper is organized as follows. The experiment setup and test conditions are described in Section 2. Section 3 gives a description of time-averaging the alongshore velocities, the spectral analysis procedures and the method of analyzing the images. Section 4 outlines the experimental results, including the velocity time series and the images of dye patch movement. In Section 5, a numerical analysis of the shear instabilities of longshore currents observed in present experiment is presented, and calculated and measured periods and wavelengths are compared. In Section 6, the dimensionless linear instability equation is used to investigate the difference between the periods for the 1:100 and 1:40 slopes, and the influences of frontshear and backshear on the calculated period. A brief discussion is included in this section. Finally, conclusions are given.

2. Experimental setup

The experiment was performed in the 55 m × 34 m × 1.0 m deep wave basin at the State Key Laboratory of Coastal and Offshore Engineering, Dalian University of Technology. The experimental layout and bottom profile are shown in Fig. 1. The beach makes an angle of 30° with respect to the wave generator, creating a large incident angle and a longer beach and allowing more room for alongshore current instability to develop. Two plane concrete profiles with 1:40 and 1:100 slopes were constructed (see Fig. 1 (lower)). The

Table 2
Test conditions and instabilities.

Case	Incident waves	Slope	D (cm)	H (cm)	T (s)	Current instability
1	Regular waves	1:100	18	3.5	1.0	Yes
2	Regular waves	1:100	18	4.5	1.0	Yes
3	Regular waves	1:100	18	2.7	1.5	Yes
4	Regular waves	1:100	18	4.2	1.5	Yes
5	Regular waves	1:100	18	3.0	2.0	Yes
6	Regular waves	1:100	18	4.5	2.0	Yes
7	Regular waves	1:40	45	5.0	1.0	Yes
8	Regular waves	1:40	45	9.4	1.0	Yes
9	Regular waves	1:40	45	12.6	1.0	Yes
10	Regular waves	1:40	45	5.9	1.5	Yes
11	Regular waves	1:40	45	10.5	1.5	Yes
12	Regular waves	1:40	45	13.0	1.5	Yes
13	Regular waves	1:40	45	5.2	2.0	Yes
14	Regular waves	1:40	45	10.0	2.0	Yes
15	Regular waves	1:40	45	13.0	2.0	Yes
16	Random waves	1:100	18	2.4	1.0	Yes
17	Random waves	1:100	18	3.9	1.0	Yes
18	Random waves	1:100	18	2.3	1.5	Yes
19	Random waves	1:100	18	5.0	1.5	Yes
20	Random waves	1:100	18	2.1	2.0	Yes
21	Random waves	1:100	18	3.4	2.0	Yes
22	Random waves	1:40	45	3.6	1.0	Yes
23	Random waves	1:40	45	5.5	1.0	Yes
24	Random waves	1:40	45	7.8	1.0	Yes
25	Random waves	1:40	45	4.0	1.5	Yes
26	Random waves	1:40	45	6.3	1.5	Yes
27	Random waves	1:40	45	9.0	1.5	Yes
28	Random waves	1:40	45	3.7	2.0	Yes
29	Random waves	1:40	45	5.7	2.0	Yes
30	Random waves	1:40	45	8.7	2.0	Yes

Note: D – still water depth, H – mean wave height, T – peak period.

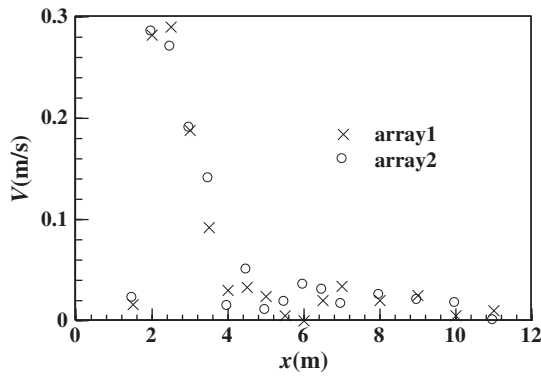


Fig. 2. Measured mean alongshore velocity for case 13 in two transects at 8 m (circles) and 12 m (crosses) from the inflow opening.

still-water depth over the horizontal bottom was 0.45 m for the 1:40 slope experiments and 0.18 m for the 1:100 slope experiments.

A wave generator consisting of individual wave paddles was located at the offshore end of the basin, having a total length of 24.5 m. The paddles were moved in phase in the present experiments.

It was decided not to recirculate the longshore current using a pump system in these experiments since it was considered that inherent difficulties in controlling the pump discharge may have influenced shear instability measurements (although not the mean longshore currents). Hence, in order to produce uniform alongshore currents recirculating in the wave basin, a circulation channel was constructed around the beach, 3.0 m wide at each end of the beach and 1.0 m deep (as in the basin where the bottom was horizontal).

To observe the oscillation motions visually and spatially, a dye-release experiment was conducted as the longshore currents were generated. The dye (ink, in this case) was continuously released in the surf zone using a long, thin tube 0.8 cm in diameter. The dye-release points were located at $x = 3$ m, $y = 8$ m and $x = 4.5$ m, $y = 8$ m for the 1:40 and 1:100 slopes respectively, and approximately one-third of the water depth from the bottom. The image of the dye patch was recorded by a CCD suspended about 10 m above the basin.

In the experiment, the free surface elevations were measured by 40 capacity-type wave gages deployed in three arrays normal to the shoreline. A total of 32 two-dimensional velocity meters (VMs) in two identical arrays of 16 (see Fig. 1) measured the flow field at a sampling rate of 20 Hz. These VMs were set at one-third of the water depth from the bottom (see Fig. 1), which is approximately the depth at which depth-averaged alongshore currents occur. The distance of the VMs from the shoreline, x , is given in Table 1. The strain-type velocity meters used are suitable for long-period horizontal oscillations (> 2 s) and for measuring long-period unstable alongshore currents in the present study.

Monochromatic, random, unidirectional and obliquely incident waves were generated in the experiments: see Table 2. Irregular waves were generated according to a JONSWAP spectrum with peak enhancement factor $\gamma = 2 \cdot 5$. Each test was repeated three times continually throughout the experiment in order to obtain the compelling results.

For each condition the procedure was firstly to create a uniform longshore current. The current velocities were measured for 4 min under regular waves and 8 min under irregular waves as they were generated. Next, the CCD system recorded the deformation of the dye patch as the mean longshore currents leveled off.

Fig. 2 shows the measurement results for case 13, in which the cross-shore profiles of the mean alongshore velocities are compared for the two VM arrays. It can be seen that the two profiles are similar, indicating that the mean alongshore currents were approximately uniform.

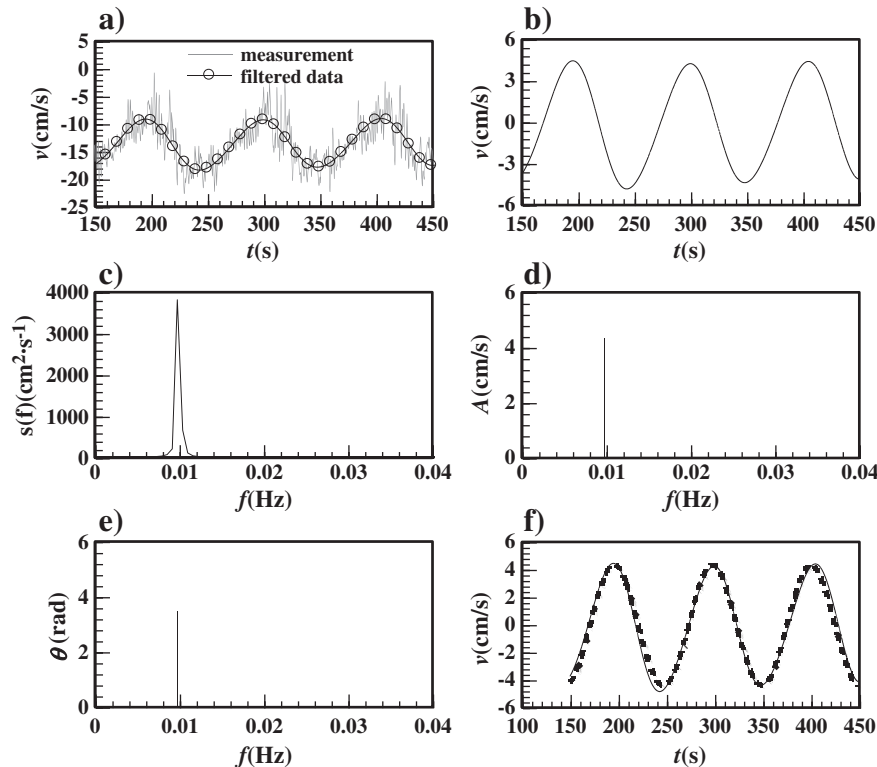


Fig. 3. (a) Measurements and filtered time series; (b) de-meaned and de-trended data (—); (c) maximum entropy spectrum; (d) amplitude spectrum A_k ; (e) phase spectrum θ_k ; (f) calculated time series of oscillation currents using A_k and θ_k (- - -).

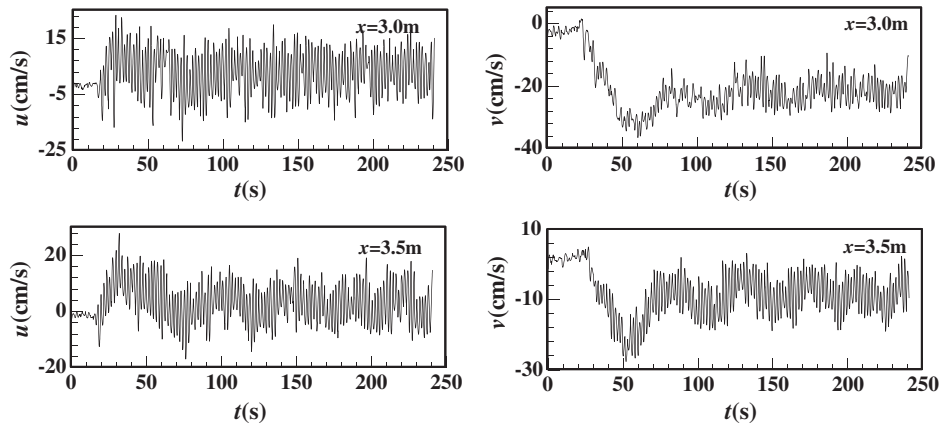


Fig. 4. Time series of cross-shore velocity u (left) and alongshore velocity v (right) for case 13 (regular waves, 1:40 slope) (x is the distance from the still-water shoreline).

3. Data analysis

This section describes the process of time-averaging alongshore velocities in order to obtain the alongshore current profiles, the spectral analysis procedures used to analyze data obtained from the alongshore array of VMs, and the method of analyzing the images. Our goal was to describe varying shear instabilities of approximately longshore-uniform coasts having essentially depth-uniform longshore currents (Sancho, 1998). Although cross-shore currents within the wave-breaking region have pronounced depth variation, linear instability theory assumes depth-averaged currents. Thus, a depth-uniform approximation for the horizontal currents was adopted in the present study, as in the other models described earlier. Spectral analysis based on the maximum entropy method (MEM) was performed in the frequency domain, and shear wave oscillation amplitudes were simultaneously derived by trigonometric regression in order to analyze the variation in shear wave energy for the cross-shore direction. The spectral analysis shows how much energy is present in a specific frequency bandwidth. However, this does not necessarily imply that the observed energy in the low-frequency bandwidths is due to shear instability, but may instead be caused by shear instability resonance.

Given that the phase speed of shear instabilities is much lower than the phase speed associated with (infra-)gravitational waves, the deformation and motion of the dye patch in the longshore direction showed whether or not the observed wave energy was due to the presence of shear instabilities. The CCD images were used to obtain the propagation speed of the dye patch by measuring the movement of fixed points (such as the peak) on the dye patch in the longshore direction with respect to time, and then fitting this data linearly. The

deformation characteristics of the dye patch are described solely from observation of the images.

3.1. Spectral analysis

Many studies have identified the shear instability of longshore currents using frequency–wavenumber spectrum analysis (e.g. Dodd et al., 1992; Noyes et al., 2004; Oltman-shay et al., 1989; Özkan-Haller and Kirby, 1999). In the present experiment only two arrays of velocity meters were set up in the alongshore direction, as a result of which the frequency–wavenumber spectrum could not be readily obtained; therefore only the frequency domain spectrum was analyzed. To compensate for this, the dye dispersion results were used to study the spatial structures of the shear waves.

Spectral analysis by the maximum entropy method (MEM) (Burg, 1967) was used to determine the dominant frequencies of the recorded time series of longshore current velocities, which were sampled at 0.05 s intervals for both regular and irregular wave conditions. Before carrying out spectral analysis, the velocity records were all intercepted from approximately 150 s to 450 s. This range was chosen because obvious alongshore currents were observed after approximately 150 s, and the filtered data did not agree well with original data beyond 450 s. Low-pass filtering was then applied to the data with threshold frequencies of 0.02 Hz for irregular waves and 0.04 Hz for regular waves. The filtered data was then de-meant and de-trended; in this study, de-trending involved removing the linear trends from the signals. Fig. 3(a)–(c) shows the above steps as an example.

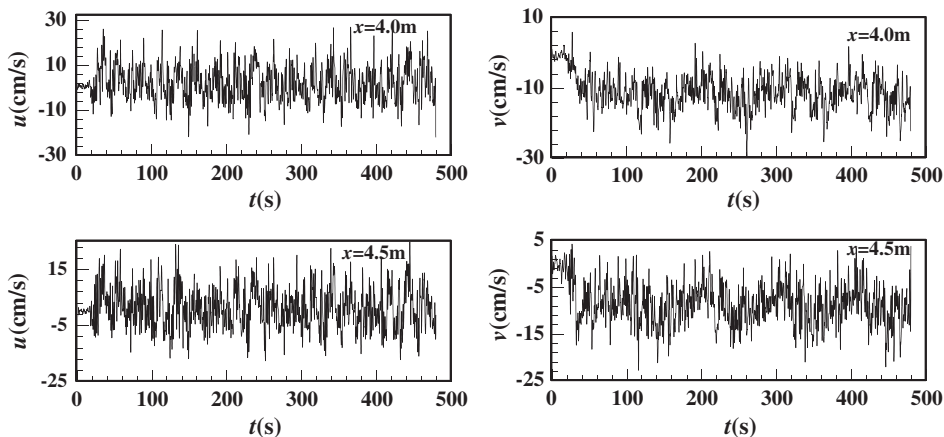


Fig. 5. Time series of cross-shore velocity u (left) and alongshore velocity v (right) for case 26 (irregular waves, 1:40 slope) (x is the distance from the still-water shoreline).

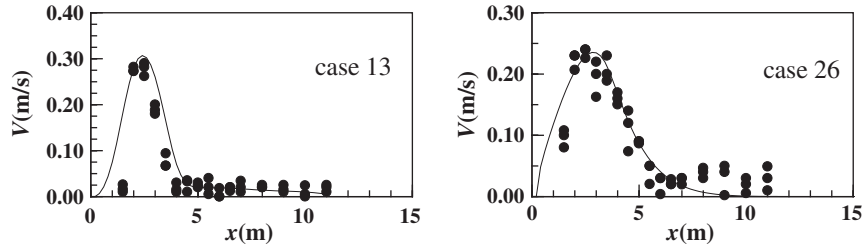


Fig. 6. Mean longshore currents for case 13 (regular waves, 1:40 slope) and case 26 (irregular waves, 1:100 slope). •: data; —: fitted curve.

3.2. Amplitudes

Amplitude estimation by MEM is not very reliable (Kane, 1999; Kane and Trivedi, 1982; Sawada et al., 1997) and was used only to determine peak frequencies f_l ($l = 1$ to m). To determinate oscillation amplitudes, the trigonometric function regression method was adopted, as set out below. If A_l and θ_l denote the amplitude and phase of the oscillations, and f_l denotes the dominant frequency of the corresponding spectrum, the filtered time series $X(t)$ may be expressed by:

$$X(t) = \sum_{l=1}^m A_l \cos(2\pi f_l t + \theta_l) \quad (1)$$

The time variable in Eq. (1) is discretized in the usual manner, i.e. $t = (i-1)\Delta$ ($\Delta = 0.05s$), where i is an integer.

$$\begin{aligned} X(i\Delta) &= \sum_{l=1}^m A_l \cos(2\pi f_l i\Delta + \theta_l) \quad (i = 0, 1, 2, \dots, N) \\ &= \sum_{l=1}^m [Y_l \cos(2\pi f_l i\Delta) + Y_{l+m} \sin(2\pi f_l i\Delta)] \end{aligned} \quad (2)$$

Hence Eq. (2) can be expressed as:

$$aY = X \quad (3)$$

where:

$$a = \begin{pmatrix} 1 & 1 & \dots & 1 & 0 & 0 & \dots & 0 \\ \cos 2\pi f_1 \Delta & \cos 2\pi f_2 \Delta & \dots & \cos 2\pi f_m \Delta & \sin 2\pi f_1 \Delta & \sin 2\pi f_2 \Delta & \dots & \sin 2\pi f_m \Delta \\ \cos 2\pi f_1 2\Delta & \cos 2\pi f_2 2\Delta & \dots & \cos 2\pi f_m 2\Delta & \sin 2\pi f_1 2\Delta & \sin 2\pi f_2 2\Delta & \dots & \sin 2\pi f_m 2\Delta \\ \dots & \dots \\ \cos 2\pi f_1 n\Delta & \cos 2\pi f_2 n\Delta & \dots & \cos 2\pi f_m n\Delta & \sin 2\pi f_1 n\Delta & \sin 2\pi f_2 n\Delta & \dots & \sin 2\pi f_m n\Delta \end{pmatrix}$$

$$X = (X_0, X_1, \dots, X_n)^T, Y = (Y_1, Y_2, \dots, Y_{2m})^T$$

$$Y_l = A_l \cos \theta_l, Y_{l+m} = -A_l \sin \theta_l \quad (l = 1, 2, \dots, m)$$

We wish to determine Y such that

$$\|aY - X\| = \min \quad (4)$$

where $\|\cdot\|$ indicates the Euclidean norm. If Q is an orthogonal matrix, the relationship is:

$$\|aY - X\|_2 = \|QaY - QX\|_2 \quad (5)$$

hence:

$$\|aY - X\| = \min \|QaY - QX\| \quad (6)$$

Eq. (4) can be solved easily for Y using QR decomposition (Golub and Van Loan, 1996):

$$Qa = \begin{pmatrix} R \\ 0 \end{pmatrix} \quad (7)$$

where Q is an orthogonal matrix and R is an upper triangular matrix. The decomposition of Eq. (7) is via Householder transformations (Householder, 1958).

$$\|QaY - QX\|_2 = \left\| \begin{pmatrix} R \\ 0 \end{pmatrix} - \begin{pmatrix} C \\ D \end{pmatrix} \right\|_2 \quad (8)$$

where $C = Q \times (X_0, X_1, \dots, X_{2m-1})^T$, $D = Q \times (X_{2m}, X_{2m+1}, \dots, X_n)^T$. Therefore:

$$\|aY - X\|_2 = [(RY - C)^T (RY - C) + D^T D]^{\frac{1}{2}} \quad (9)$$

When $Y = R^{-1}C$, the left-hand side of Eq. (9) takes a minimum value, satisfying Eq. (4). Y can then be obtained easily. Then A_l and θ_l

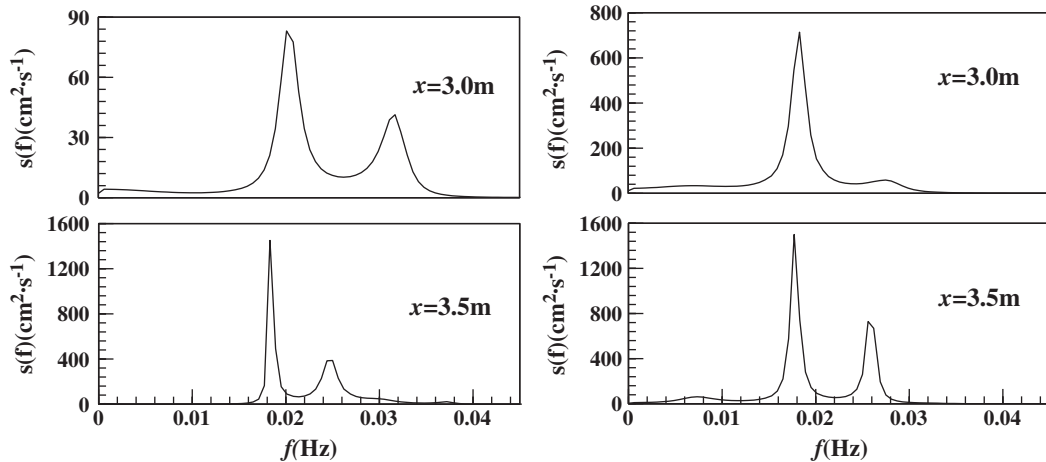


Fig. 7. Spectra at $x = 3$ m and $x = 3.5$ m corresponding to the recorded time series in Fig. 4 for case 13 (regular waves, 1:40 slope).

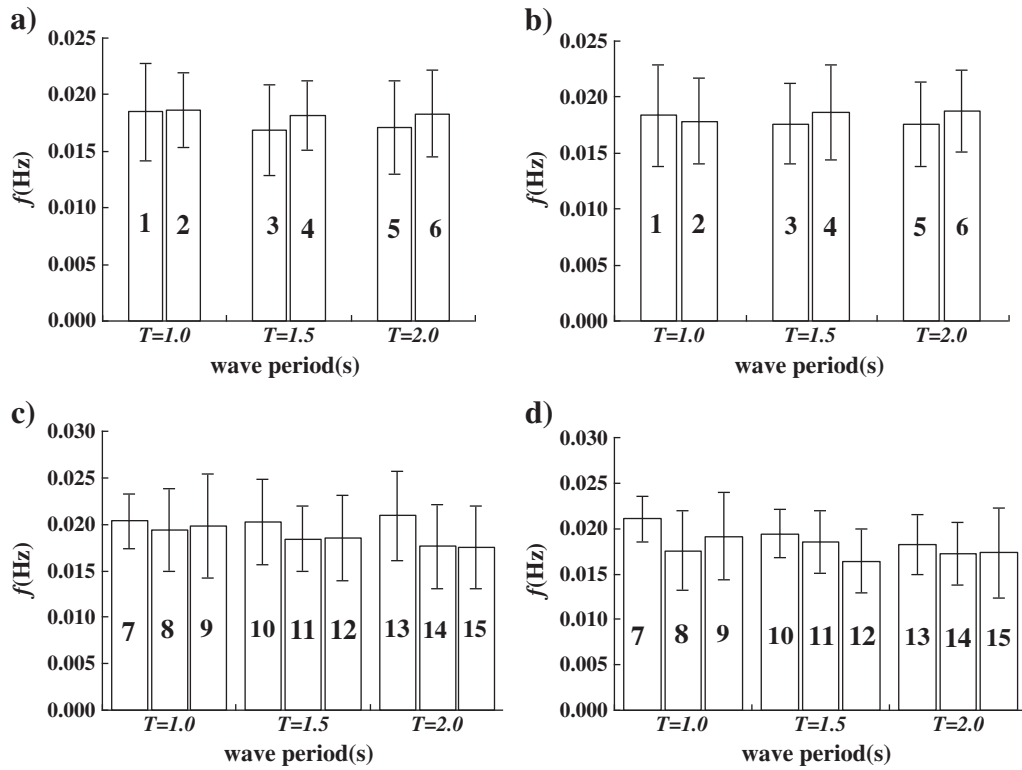


Fig. 8. (a) Averaged dominant frequencies of shear waves in cross-shore for cases 1–6; (b) alongshore for cases 1–6; (c) averaged dominant frequencies of shear waves in cross-shore for cases 7–15; (d) alongshore for cases 7–15. The number in the box denotes the test condition number. The results for regular wave cases (1:100 slope) are given in (a) and (b); (c) and (d) are for regular waves (1:40 slope).

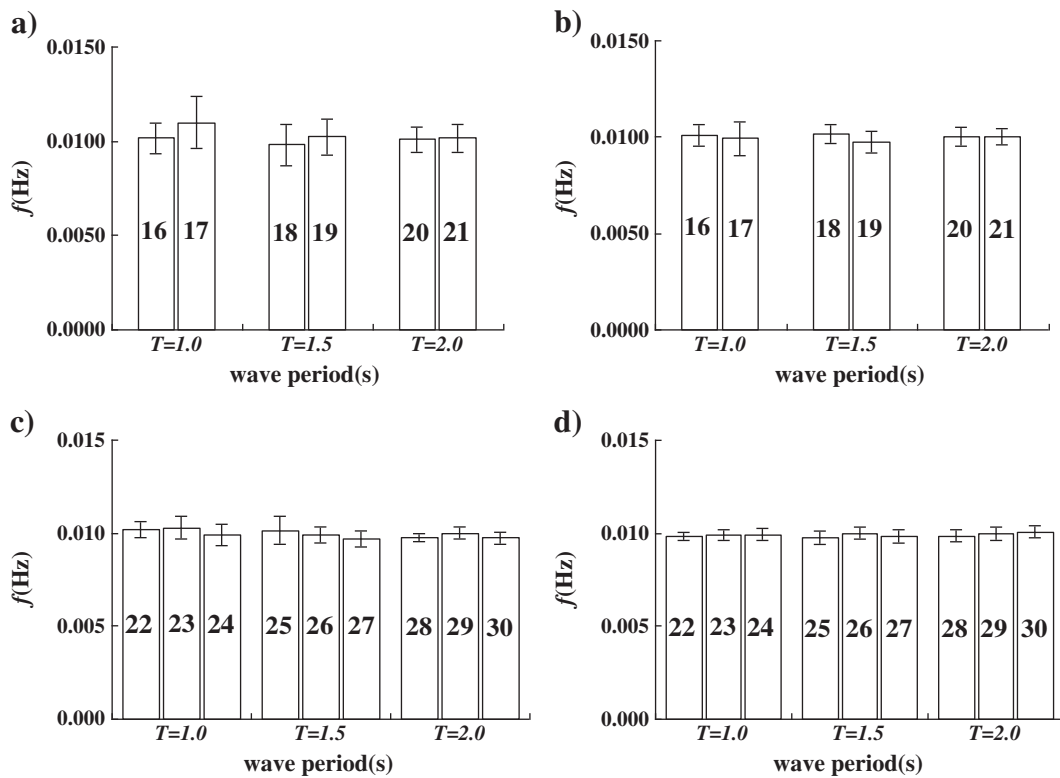


Fig. 9. (a): Averaged dominant frequencies of shear waves in cross-shore for cases 16–21; (b) alongshore for cases 16–21; (c) averaged dominant frequencies of shear waves in cross-shore for cases 22–30; (d) alongshore for cases 22–30. The number in the box denotes the test condition number. The results for irregular wave cases (1:100 slope) are given in (a) and (b); (c) and (d) for irregular waves (1:40 slope).

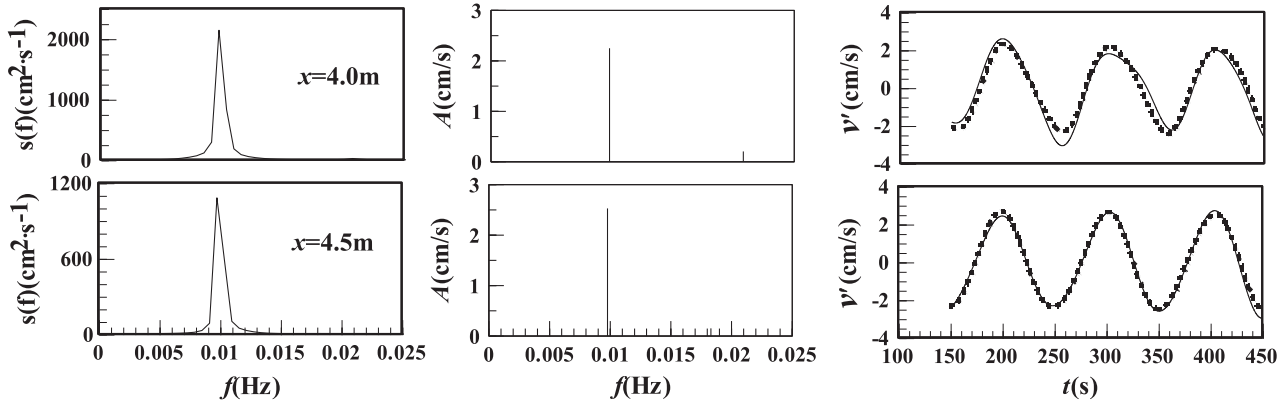


Fig. 10. Spectra of the alongshore velocity time series (from $x = 2$ m to $x = 4.5$ m) (left); calculated amplitudes corresponding to selected peaks in spectra (center); de-meaned and de-trended time series (—) and the calculated time series (---) (right) for case 26 (irregular waves, 1:40 slope).

can be obtained from:

$$A_l = \sqrt{Y_l^2 + Y_{m+l}^2}; \theta_l = \arctg\left(-\frac{Y_{l+m}}{Y_l}\right)$$

The frequency number depends on the spectrum: for instance, a single peak appears in Fig. 3(c), hence $m = 1$. Fig. 3(d) and (e) shows A_l and θ_l as corresponding to the frequency 0.00977 Hz. This method was used to calculate the oscillation amplitudes (u' , v') corresponding to the dominant frequency.

3.3. Propagation speeds of shear waves

As mentioned above, the spectral analysis does not imply that the observed energy in the low-frequency bandwidths is due to the presence of shear instabilities. Therefore quantitative analysis is necessary to identify and investigate the characteristics of the shear instability of longshore currents. In the following, the estimation method of the propagation speeds of the shear instability is given.

The CCD images were used to determine shear wave propagation speed, obtained by measuring the movement distance over time of the crest or trough of a dye patch from the measurement beam location. Its actual location does not affect the analysis results.

4. Results

4.1. Frequency domain

To check the shear instabilities, a spectral analysis in the frequency domain has been done for all the time series obtained by the current velocity meters in the cross-shore array for longshore velocity (similar results were obtained for the cross-shore velocity). For brevity, attention is focused on the results for case 13 (regular waves), case 21 (irregular waves, 1:100 slope) and case 26 (irregular waves, 1:40 slope). Similar results were obtained for other tests.

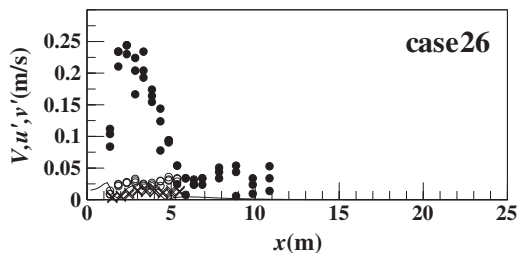


Fig. 11. Amplitudes of oscillation velocity (u' , v'). •: mean alongshore current; ×: u' ; ◊: v' ; —: calculated v' using Eqs. (12) and (13) for case 26 (irregular waves, 1:40 slope).

Figs. 4 and 5 show the recorded time series of cross-shore (left) and alongshore currents (right) velocities for case 13 (regular waves, Fig. 4) and case 21 (irregular waves, Fig. 5). Large-amplitude, long-period oscillations were clearly present in both the alongshore and cross-shore velocity components; these were also observed to occur under all test conditions, with a period of approximately 50 s for regular waves and 100 s for irregular waves. It can be seen that the long-period oscillations were more regular for the irregular waves than for the regular waves. Fig. 6 gives the measured mean longshore currents for case 13 (regular waves) and case 21 (irregular waves). The solid curves fitted to the results, shown in both figures, were used as input data for the linear instability analysis in Section 5.

It was noted above that the approximate oscillation periods were estimated from the recorded velocity time series. In order to rigorously investigate the way in which the observed oscillation periods varied with test conditions, it was necessary to determine the dominant oscillation frequencies by spectral analysis of the frequency domains as described below.

4.2. Dominant frequencies of shear waves for regular wave cases

Fig. 7 gives the results of the spectral analysis for the cross-shore and alongshore velocity at $x = 3$ m and $x = 3.5$ m for case 13; a distinct peak can be seen at approximately 0.02 Hz in both spectra. Because the amplitudes estimated using MEM was found to be unreliable, the method was used only for detecting the dominant peak. Hence the existence of distinct peaks in the spectra of the cross-shore and alongshore velocities in Figs. 7 and 10 was explained using the amplitude spectrum obtained by trigonometric function regression. For example, the amplitudes at frequencies of 0.025 Hz and 0.032 Hz in Fig. 7 are very small, possibly due to nonlinear interaction or related to the location of the current meter; hence 0.02 Hz has been regarded as the dominant frequency. Similarly, it can be seen that the amplitude corresponding to 0.02 Hz in Fig. 10 was very small but was considerable at 0.01 Hz; the dominant frequency was therefore taken to be 0.01 Hz. The dominant frequencies were considered to be those at which the mean longshore current velocity exceeded the maximum mean longshore current by 20% or more for each case. The average of these was then adopted as the dominant frequency for each case, and its standard deviation was then determined. Fig. 8(a) and (b) shows the average and standard deviation of dominant frequencies in the cross-shore (T_x) and alongshore (T_y) directions for the 1:100 slope (regular wave conditions) and Fig. 8(c) and (d) for the 1:40 slope (regular wave conditions). In Fig. 8 the dominant frequency is seen to be approximately 0.02 Hz for regular waves. Wave height, period and beach slope all had a negligible effect on the dominant frequency; the standard deviation of the dominant frequency for all cases, for both slopes, was ± 0.005 Hz.

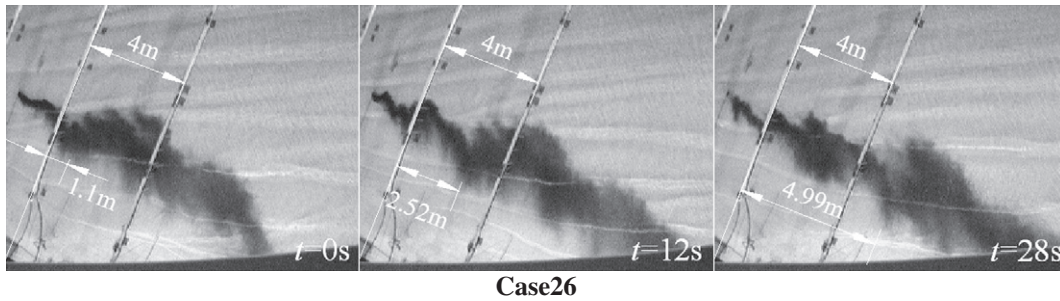


Fig. 12. Measurements of the displacements of dye patch crests for case 26.

4.3. Dominant frequencies of shear waves for irregular wave cases

Similarly for irregular waves, frequency domain analysis was performed by the maximum entropy method to determine the dominant frequencies of the recorded time series of the longshore current. The time series of alongshore velocities was sampled at intervals of 0.05 s over 480 s for irregular wave conditions.

Fig. 9(a) and (b) shows the average and standard deviation of the dominant frequencies in the cross-shore (T_x) and alongshore (T_y) directions for the 1:100 slope (irregular wave conditions) and Fig. 9(c) and (d) for the 1:40 slope (irregular wave conditions). In Fig. 9 the dominant frequency is seen to be approximately 0.01 Hz for irregular waves. Wave height, period and beach slope all had a negligible effect on the dominant frequency. The standard deviation of the dominant frequency for irregular waves was significantly smaller than for regular waves, which suggests that shear instability in longshore currents was produced much more readily for irregular waves than for regular waves. This conclusion agrees with that of Renier (1997). In particular, the standard deviation of the dominant frequency for all cases for the 1:100 slope was larger than for the 1:40 slope in both the cross-shore and alongshore directions for irregular waves. This may have been due to shoaling and the much stronger nonlinear influence of the 1:100 slope.

4.4. Oscillation amplitudes of shear waves for irregular waves

Variations in the oscillation strength in the cross-shore direction were analyzed as follows. Analysis of this aspect, either in field or

laboratory experiments on longshore current instability, has not previously been reported; however, it is significant for gaining an understanding of how shear instability of longshore currents modifies sediment transport and accretional erosion on beaches.

Fig. 10 shows the spectra of the alongshore velocity time series at $x=4$ m and $x=4.5$ m for calculated amplitudes corresponding to selected peaks in the maximum entropy spectra for case 26. The figure shows the de-measured and de-trended (solid line) and calculated time series (dashed line) using calculated amplitudes and phases (not shown).

Fig. 11 shows the oscillation amplitudes of u' and v' for case 26. Similar results were obtained for the other cases. The measured mean alongshore current is also given in the two figures. It is seen that the amplitude variations u' and v' in the cross-shore direction are similar to the variations in the mean alongshore currents in the cross-shore direction, and the maximum values of u' and v' are located close to the locations of the mean alongshore current maxima. The amplitude of v' is generally greater than the amplitude of u' , implying that the perturbation energy due to u' is less marked than that due to v' , having a maximum of about one-sixth of the maximum mean alongshore current. The calculated results for v' using the linear instability model are given in the figure to be discussed in Section 5.

As discussed above, shear instability was found to develop much more fully for irregular waves than for regular waves, oscillation amplitudes were larger, and longer time series were recorded. Therefore, the irregular wave oscillation amplitudes were able to be calculated much more accurately. Since the analysis of irregular wave systems is a potentially useful source of information for engineers,

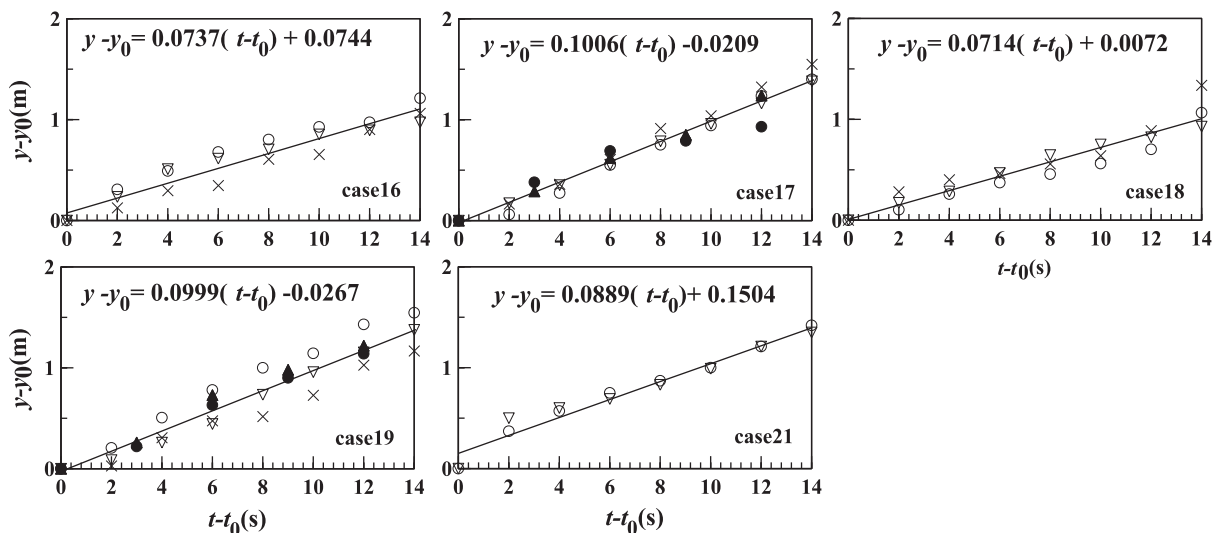


Fig. 13. Displacement of dye patch crest vs time ($\nabla \times \blacktriangle \bullet$) and its best fit line (—) for cases 16–19, 21 (irregular waves, 1:100 slope). y_0 and t_0 are position and time at start.

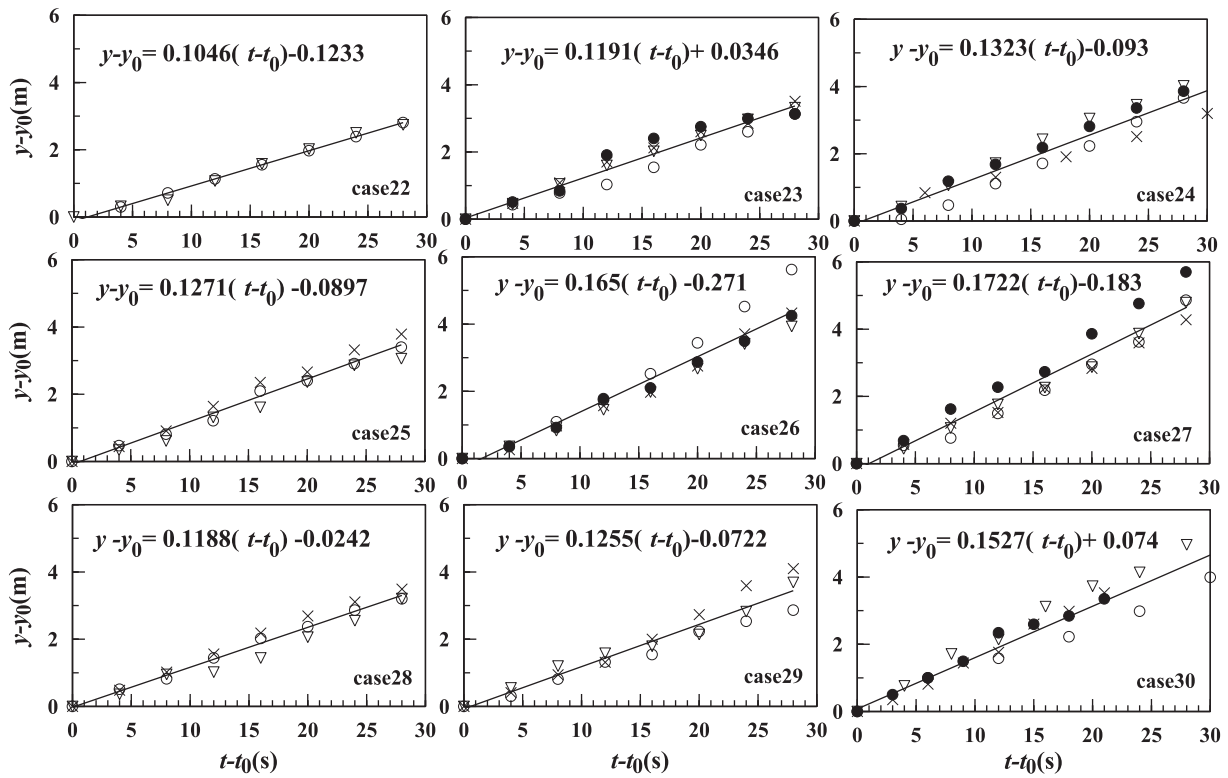


Fig. 14. Displacements of dye patch crests vs time ($\nabla \circ \times \blacktriangle \bullet$) and its best fit line (—) for cases 22–30 (irregular waves, 1:40 slope). y_0 and t_0 are position and time at start.

these observations stimulated further investigation of cross-shore oscillation amplitude characteristics.

4.5. Propagation speeds of shear waves

The dye patch was observed to move alongshore with the longshore currents, presenting as a wavy pattern in the alongshore direction. Analysis of the movement pattern was necessary in order to show that the meandering movements of the alongshore current shown in Fig. 12 are indeed due to the presence of shear waves and not to any other type of low-frequency flow. If the observed propagation speeds agree with the calculated results from linear instability theory it is reasonable to conclude that the pattern was induced by the shear instability of the alongshore currents.

The images showed that the shear instability was fully developed after 14 s for the 1:100 slope, and 28 s for the 1:40 slope. Fig. 12 presents the measurements for case 26. The dye patch was tracked at

intervals of 1 s (1:100 slope) and 2 s (1:40 slope). To estimate the propagation speed of the shear waves, the measurement results were fitted linearly; the propagation speed was then estimated from the slopes and intercepts of the linear fit.

The results of the propagation speeds obtained in this way are shown in Fig. 13 (irregular waves, 1:100 slope) and Fig. 14 (irregular waves, 1:40 slope). The ratios of the propagation speed to the maximum mean alongshore current velocity, c/V_{max} , are plotted in Fig. 15. These show that the propagation speed of the shear waves was approximately 50%–75% of the maximum mean alongshore current.

5. Numerical analysis

Bowen and Holman (1989) illustrated the mechanism for shear instability due to background vorticity. This model showed good agreement with the field observations of Oltman-Shay et al. (1989). Subsequently, most of the theoretical analysis on the shear waves has

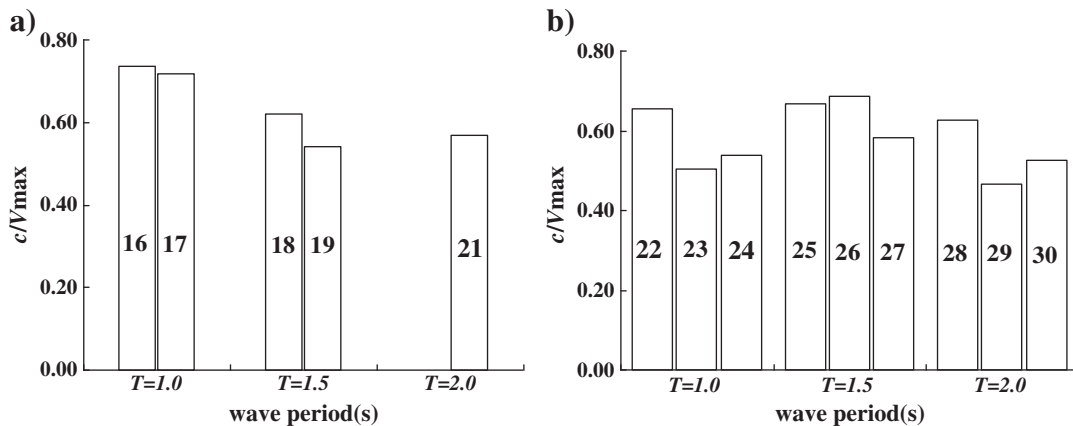


Fig. 15. Ratios of propagation speeds to maximum mean alongshore currents, c/V_{max} , for irregular waves. (a) 1:100 slope; (b) 1:40 slope.

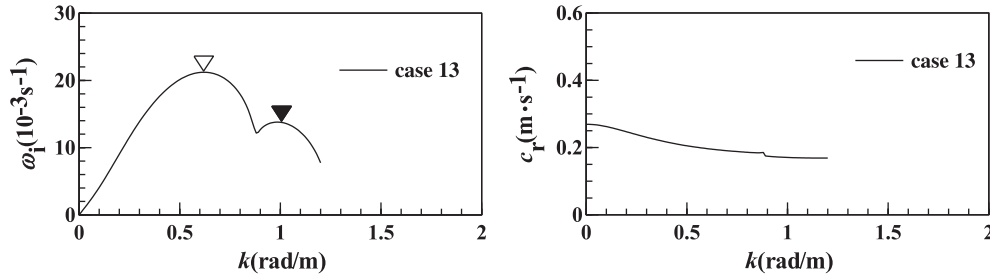


Fig. 16. Variations of growth rate, ω_i , and propagation speed, c_r , vs wave number, k . Regular waves, case 13; 1:40 slope.

essentially been based on the Bowen and Holman model, including a number of nonlinear shear wave studies (e.g. Allen et al., 1996; Slinn et al., 1998; Özkan-Haller and Kirby, 1999; Noyes et al., 2004).

In the present study, mathematical analysis of linear shear instabilities of measured mean longshore currents was compared to the theoretical results (periods of shear waves) of the spectral analysis results given above. It was assumed that the flow field can be represented by a steady longshore current $V(x)$ with small superimposed perturbations $u'(x, y) = [u'(x, y), v'(x, y)]$; that is:

$$u(x, y) = [u'(x, y), V(x) + v'(x, y)] \quad (10)$$

Bowen and Holman's (1989) theoretical model is in the form:

$$(V-c) \left(\varphi_{xx} - k^2 \varphi - \frac{\varphi_x h_x}{h} \right) - h \varphi \left(\frac{V_x}{h} \right)_x = 0 \quad (11)$$

where the perturbation velocities take the forms:

$$u' = -\frac{\psi_y}{h} = -\frac{i\varphi k}{h} \exp(\omega_i t) \exp(i(ky - \omega_r t)) \quad (12)$$

$$v' = \frac{\psi_x}{h} = \frac{\varphi_x}{h} \exp(\omega_i t) \exp(i(ky - \omega_r t)). \quad (13)$$

This model was applied to analyze the instability in the present experiment.

It is well known that the necessary condition for the occurrence of instability is the presence of an inflection point in the velocity profile. If the inflection point occurs at the back side (seaward side) of the velocity profile, the instability is termed the 'backshear' mode; the 'frontshear' mode then occurs at the front side (shoreward side) of the velocity profile (Baquerizo et al. 2001). In the present study, the theoretical and experimental results show that the observed oscillations for the different beach slopes were related to different instability models: backshear instability for the 1:40 slope and frontshear for the 1:100 slope.

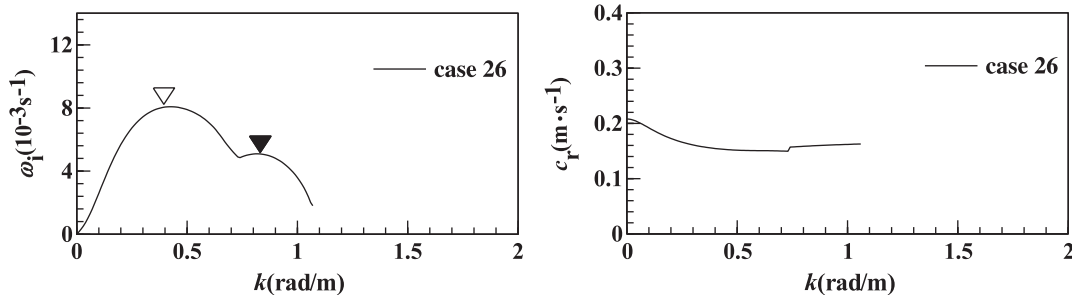


Fig. 17. Variations of growth rate, ω_i , and propagation speed, c_r , vs wave number, k . Irregular waves, case 26; 1:40 slope.

5.1. Theoretical calculation results for 1:40 slope

The velocity profiles of the mean longshore currents (fitted results) for the 1:40 slope (such as case 13 shown in Fig. 6) were adopted as the background shear flows in the linear instability analysis, with the fitted lines in place of the discrete test data. Figs. 16 and 17 show the growth rate, ω_i , and the propagation speed, c_r , of the shear waves vs wave number k for cases 13 and 26 for the 1:40 slope. It is seen in both figures that there are two peaks: the first corresponding to the backshear mode, and the second to the frontshear mode; however, there is only one peak growth rate for different values of k , and this corresponds to the backshear mode for other cases. For cases 13 and 26, the wave number, k_0 , corresponding to the maximum growth rates, the corresponding propagation speed, c_r , and period ($T = 2\pi(k_0 c_r)^{-1}$) of the shear waves are given in Table 3. The experimental results for T_x and T_y , the dominant periods of the shear waves obtained from the cross-shore and alongshore velocity time series, are also given in the table. The calculated periods corresponding to the backshear mode agree with the experimental results – that is, around 50 s for regular waves (cases 7–15) and around 100 s for irregular waves (cases 22–30), implying a backshear mode for the observed shear waves for the 1:40 slope. The reason for the smaller oscillating period for regular wave cases may be due to the narrow mean velocity profiles for the regular wave cases leading to slow variation of shear, V_x , in the mean longshore current. V_x is the dominant characteristic of the unstable longshore current in terms of the linear instability theory. That is to say that the shear, V_x , acts in the same way as the Coriolis effect, f .

5.2. Theoretical calculation results for 1:100 slope

From similar analyses for the 1:100 slope, Figs. 18 and 19 show ω_i and c_r vs k shear waves for cases 3 and 19 for the 1:100 slope. Both figures show two modal peaks for the two cases (similar results were obtained for other cases), the first corresponding to backshear, and the second to frontshear. Table 4 lists wave number, k_0 , corresponding to the maximum growth rates, the corresponding propagation speed, c_r , and period ($T = 2\pi(k_0 c_r)^{-1}$) of the shear waves. As in Table 4, the experimental results of the dominant period of shear waves obtained

Table 3

Numerical results for shear waves for 1:40 slope (cases 7–15: regular waves; cases 22–30: irregular waves).

Case	Backshear mode				Frontshear mode				Exp.		
	k_{01}	c_{r1}	T_1	L_1	k_{02}	c_{r2}	T_2	L_2	c_e	T_x	T_y
7	0.70	0.176	51.00	8.97	1.39	0.155	29.21	4.52	0.1313	49.23	47.53
8	0.45	0.242	57.66	13.96	0.90	0.219	32.01	6.98	0.194	49.32	51.47
9	0.58	0.202	53.56	10.83					0.2861	47.84	54.77
10	0.55	0.187	61.06	11.42					0.1714	51.65	56.89
11	0.45	0.213	65.41	13.96					0.3089	54.31	54.09
12	0.51	0.201	61.32	12.31					0.2786	56.70	57.92
13	0.62	0.195	51.89	10.13	0.99	0.171	37.10	6.34	0.1273	50.43	52.26
14	0.63	0.220	45.31	9.97					0.1419	54.03	60.85
15	0.34	0.291	63.47	18.47	0.70	0.264	33.98	8.97	0.1917	57.31	57.75
22	0.520	0.120	100.64	12.08					0.1046	98.17	101.54
23	0.360	0.167	104.46	17.44					0.1191	97.24	100.91
24	0.370	0.174	97.55	16.97					0.1323	100.68	100.74
25	0.570	0.115	95.81	11.02					0.1271	98.60	102.32
26	0.420	0.154	97.09	14.95					0.1650	101.20	99.94
27	0.340	0.212	87.13	18.47	0.90	0.221	31.57	6.98	0.1722	103.04	101.92
28	0.660	0.103	92.38	9.52					0.1188	102.34	101.47
29	0.370	0.181	93.77	16.97					0.1255	99.94	100.21
30	0.300	0.183	114.56	20.93					0.1527	102.72	99.26

Note: k_0 is the wave number corresponding to the maximum growth rate; c_r is the propagation speed corresponding to k_0 ; $T_1 = 2\pi(k_0 c_r)^{-1}$; Exp. denotes experimental results.

from the cross-shore and alongshore velocity time series, T_x and T_y , are also given. The calculated periods corresponding to the frontshear mode agree with the experimental results, which, as in Table 4, are around 50 s and 100 s for regular and irregular waves respectively. This implies that the shear waves observed for the 1:100 slope were frontshear mode, unlike the 1:40 slope where the experimental results correspond to backshear modes, as discussed above. This may be due to the greater width of the surf zone in the case of the 1:100 slope.

5.3. Comparison of shear wave propagation speeds

The observed propagation speeds of the shear waves for irregular wave cases presented in Figs. 13 and 14 were further examined by comparing the calculated and measured values set out in Tables 3 and 4. The comparison shows that the calculated results, including the period (T_y , the dominant frequency in the alongshore direction, which is taken as the dominant shear wave frequency, and which the results show to be similar in value to T_x) and the propagation speed both agree with measured results, and also confirm the results of the theoretical analysis – that is, that the observed shear waves were indeed the backshear modes for the 1:40 slope and the frontshear modes for the 1:100 slope.

6. Discussion

As mentioned above, the calculated periods for the backshear instability mode are in agreement with the observed data. It is suggested that the backshear of the mean longshore currents velocity profile plays an important role in producing the observed shear

instability of the longshore currents for the 1:40 slope. However, it was shown that much more attention should be paid to the frontshear mode when comparing the calculated periods and propagation speeds of shear waves with the experimental results for the 1:100 slope, since the calculated periods for the backshear are approximately double those for the frontshear.

In attempting to analyze these observations, firstly it was noticed that the results varied with beach slope; therefore we examined theoretically the sensitivity of the calculated period of the shear waves to variation in slope. The effect of the different velocity profiles on the results of the linear instability analysis were then investigated, taking into account the fact that it was known from other research that the instability mode is sensitive to the mean longshore current profile. This work is significant for the understanding and analysis of the observations in the present experiments. It is acknowledged that the measurements of longshore currents near the shoreline and at the tail of the seaward velocity profile were not sufficiently accurate due to their nonlinearity, the limited deployment of velocity meters, and the assumption of uniform depth. In essence, therefore, the fitted curves of the mean longshore current velocities may be not unique; thus the influences of experimental limitation and the assumption of uniform depth on the theoretical analysis need to be investigated by examining what the effect would be if the velocity profiles were changed. Finally, the effects of regular and irregular waves on the shear wave periods are discussed.

6.1. Effects of the plane slope on shear instability

It has been shown that all the velocity profiles have an inflection point at the back side of the velocity profile (the extremum of

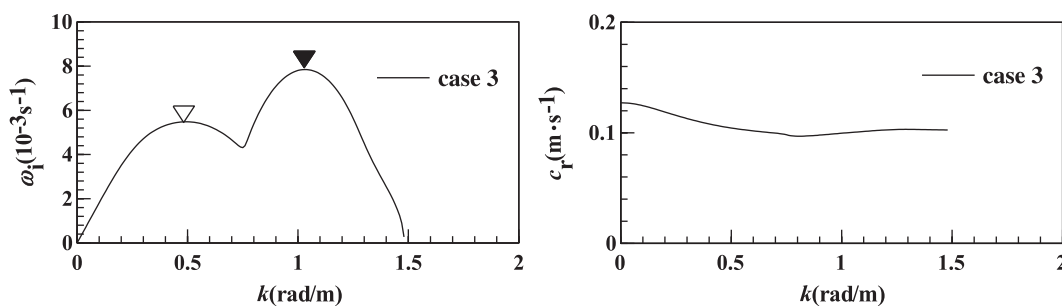


Fig. 18. Variations of growth rate, ω_i , and propagation speed, c_r , vs wave number, k for cases 1–6 (regular waves, 1:100 slope).

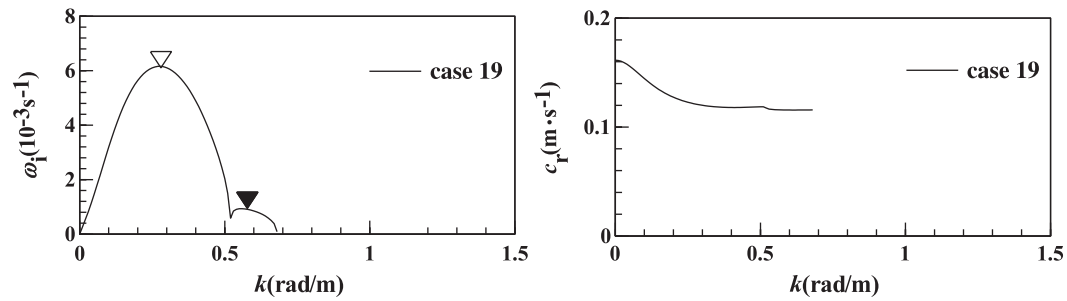


Fig. 19. Variations of the growth rate, ω_i , and propagation speed, c_r , vs wave number, k , for cases 16–21 (irregular waves, 1:100 slope).

background vorticity) and all the corresponding velocity profiles have a maximum (dominant) growth rate which corresponds to the backshear mode of shear instability (see Fig. 16–19). It was also noted that while the periods obtained from the backshear modes for the 1:40 slope agree with the observed periods of shear waves it is not true of the 1:100 slope, suggesting that beach slope has a considerable effect on the backshear modes.

In order to analyze the effects of mean longshore current profiles on backshear modes for constant frontshear mode, only those fitted velocity profiles displaying an inflection point at the back side of the velocity profile were chosen for this purpose: cases 17, 19 and 21 for the 1:100 slope, and cases 22, 25 and 28 for the 1:40 slope. These were nondimensionalized by the following relations:

$$\begin{aligned} h' &= h/h_b, & x' &= x/x_b, & V' &= V/V_0, & c' &= c/V_0, \\ k' &= kx_b, & \varphi' &= \varphi/(V_0x_b), \end{aligned} \quad (14)$$

where the prime denotes a dimensionless variable; x_b is the distance from the wave breaking point to the shoreline; h_b is the water depth at x_b ; and V_0 is the maximum mean longshore current. The nondimensional method of analysis was adopted for the reason that the beach slope vanishes from the equation after nondimensionalization. Table 5 lists x_b and h_b for all six cases. Since the wave heights and periods of cases 17 vs 22, 19 vs 25 and 21 vs 28 are similar, the nondimensional velocity profiles for each pair of experimental cases are also similar, as shown in Fig. 20. Therefore, for each pair of nondimensional velocity profiles, the test conditions differ only in the slope of the beach. Then, by comparing the calculated curves of linear instability, the effects of slope on the backshear mode were investigated. To nondimensionalize Eq. (11) using the transformation (14), the relations (14) are substituted into Eq. (11), thus expressing the equation in nondimensional variables in the same form as Eq. (11) for the plane beach ($h = \alpha x$, where α is the beach slope, and x is the distance from the shoreline).

Since, as discussed above, the beach slope vanishes from the nondimensional governing equation, which has the same form as the dimensional equation, the shear wave solutions for both the 1:100 and 1:40 slopes then depend only on the nondimensional mean longshore current velocity profiles. By examining the difference between the resultant corresponding shear wave periods, the effect of the different slopes can be seen for the three pairs of velocity profiles under corresponding test conditions of wave period and height. From the solutions to the nondimensional counterpart of Eq. (11) using these nondimensional velocity profiles as background shear, the nondimensional wave number k'_0 corresponding to the maximum growth rate, the nondimensional propagation speed c'_r corresponding to k'_0 and the corresponding nondimensional period $T' = 2\pi/(k'_0c'_r)$ were obtained, as shown in Table 6. Using the transformation (14), the corresponding dimensional period $T = 2\pi[(k'_0/x_b)c'_rV_0]^{-1} = (T'x_b)/V_0$ was obtained, as also shown in the table.

Table 5 shows that the differences of the nondimensional period T' are small when comparing cases 17 and 22, 19 and 25, and 21 and 28. Considering that the slopes are different for the two cases in each pair of velocity profiles, this small difference confirms that the beach slope has no effect on the nondimensional results of linear instability: that is, similarity in the nondimensional velocity profiles leads to similar nondimensional numerical values. However, the last column of Table 5 contains differing values for corresponding dimensional periods. For example, the dimensional period for the 1:100 slope is approximately twice that for the 1:40 slope. This is due to the different surf zone width x_b and water depth h_b for the two slopes. The former is approximately twice the latter (V_0 is similar due to the similar wave height and period for the two cases). This demonstrates that the different beach slopes led to different periods of shear wave if one instability mode only (the backshear mode) occurred for the present cases. As given in Section 3, the observed periods of shear waves for the 1:100 and 1:40 slopes are almost the same: around 50 s for regular waves and around 100 s for irregular waves. The results in Table 5, however, show that, for the 1:100 slope, the oscillating periods of

Table 4
Numerical results of shear waves for 1:100 slope (cases 1–6: regular waves; cases 16–21: irregular waves).

Case	First mode				Second mode				Exp.		
	k_{01}	c_{r1}	T_1	L_1	k_{02}	c_{r2}	T_2	L_2	c_e	T_x	T_y
1	0.41	0.112	136.30	15.32	0.90	0.110	63.43	6.98	0.0832	54.15	54.48
2	0.45	0.126	111.17	13.96	0.91	0.133	52.08	6.90	0.0968	53.72	56.07
3	0.49	0.105	122.41	12.82	1.03	0.100	60.93	6.10	0.0975	59.30	56.85
4	0.24	0.135	194.11	26.17	0.76	0.131	63.08	8.26	0.1162	55.04	53.67
5	0.39	0.099	163.30	16.10	1.05	0.101	59.22	5.98	0.1088	58.59	56.83
6	0.58	0.100	109.02	10.83	0.98	0.126	50.86	6.41	0.1115	54.61	53.34
16	0.460	0.062	218.92	13.65	0.990	0.054	116.88	6.34	0.0737	98.47	98.97
17	0.280	0.080	279.48	22.43	0.620	0.076	133.28	10.13	0.1006	90.93	100.81
18	0.480	0.075	174.35	13.08	1.10	0.063	90.62	5.71	0.0714	102.03	98.45
19	0.280	0.121	185.48	22.43	0.560	0.116	96.72	11.21	0.0999	97.77	102.63
20	0.340	0.076	243.83	18.47	0.790	0.073	109.25	7.95		98.92	99.48
21	0.270	0.097	239.94	23.26	0.590	0.083	128.62	10.64	0.0889	98.36	99.84

Table 5
Values of x_b , h_b and V_0 for some cases.

	Case 17	Case 19	Case 21	Case 22	Case 25	Case 28
x_b (m)	9.80	10.20	9.80	3.70	4.40	4.60
V_0 (m/s)	0.127	0.175	0.145	0.154	0.159	0.145
h_b (m)	0.098	0.102	0.098	0.0925	0.110	0.115

shear waves corresponding to the backshear mode do not agree with the observed results, although they are dominant for both the 1:100 and 1:40 slopes. This conclusion confirms that the observed periods of shear waves are explicable in terms of the frontshear mode for the 1:100 slope cases only, as discussed in Section 4.

6.2. Effects of velocity profile on frontshear instability

Baquerizo et al. (2001) discussed the longshore current instability caused by frontshear and backshear instabilities and proved the existence of frontshear instabilities due to the presence of a second extremum in the background vorticity at the front side of the longshore current. As analyzed in Section 5.2, the frontshear instability was indeed dominant in the present experiment for the 1:100 slope when the calculated periods and shear wave propagation speeds were compared to the observed results. Therefore, to some extent the investigation of the effects of velocity profile on frontshear instability is helpful to the understanding and application of the shear instability theory.

If the velocity profile has an inflection point at its front side (an extremum of background vorticity at the front side of the velocity profile), a frontshear instability mode will occur as stated by Baquerizo et al. (2001). In order to detect it, a large number of velocity meters would be required in this region but this was not the case in the present experiment; only a limited number were located in this region,

insufficient to detect the frontshear with accuracy. Hence, even if a frontshear extremum had been present during the experiment, it may not have been detected. In order to compensate for this weak point, the fitted lines for the velocity profiles of the mean longshore currents have deliberately included a frontshear extremum for the 1:100 slope. The linear instability results calculated using these velocity profiles are shown in Figs. 18 and 19. These indicate that one of the instability curves is related to the backshear mode (the first mode) since it responds to backshear changes, and the other (the second mode) is clearly associated with the existence of the frontshear since the growth rates vary with frontshear values. Using the second growth rate peak, the values of corresponding wave number, k , and propagation velocity, c_r , were obtained. The shear wave periods and wavelengths of the frontshear modes were then calculated from the relation $T = 2\pi(k_0 c_r)^{-1}$ (see Table 4). The oscillation periods and propagation speeds corresponding to the frontshear instability modes are similar to the measured results. The conclusion that the shear instability is related to frontshear instability for the 1:100 slope can also be examined by the flow structure of meandering longshore currents, as shown in Fig. 21 (case 3, regular wave) and Fig. 22 (case 19, irregular wave). The perturbation velocities were calculated from Eqs. (12) and (13). The shear wave velocity has been scaled so that its peak magnitude equals one-sixth of the peak mean longshore current, in accordance with experiment analysis results. The amplitude of v' obtained in this way is also shown in Fig. 11 (solid line), and its trend (shown as circles) agrees with the amplitude from the experiment. The corresponding patterns of dye movement recorded in the experiment for these two cases are shown in Fig. 12, in which the wavelengths in the dye pattern are seen to be similar to those of the calculated frontshear mode. In Table 4, the wavelengths of all the backshear modes are seen to be double those of the frontshear mode. From the above discussion it is suggested that the spatial scale of the frontshear mode for the 1:100 slope substantially agrees with the observed meandering longshore currents, but the backshear mode does not.

6.3. Combined effects of velocity profiles on frontshear and backshear instability

In reality, the velocity profile simultaneously influences both backshear and frontshear instability. The combined effects were evaluated by analyzing the sensitivity of the calculated periods of the shear waves to changes in the front- and backshears of the mean longshore currents.

Cases 21 (1:100 beach slope) and 27 (1:40 beach slope) were randomly chosen for nondimensional analysis. Four nondimensional velocity profiles were selected for each case and the corresponding differences between the instability analysis results analyzed using Eq. (14).

For case 27, four velocity profiles V1, V2, V3 and V4 were chosen: see Fig. 23(a). The profiles were obtained by changing the fitted curves for the mean longshore current. V1 and V2 have equal backshear but different frontshear: Fig. 23(b) shows that V1 has a frontshear peak but V2 does not. V3 and V4 have equal backshear values (different from V1 and V2) and different frontshear: V3 has the same frontshear as V2

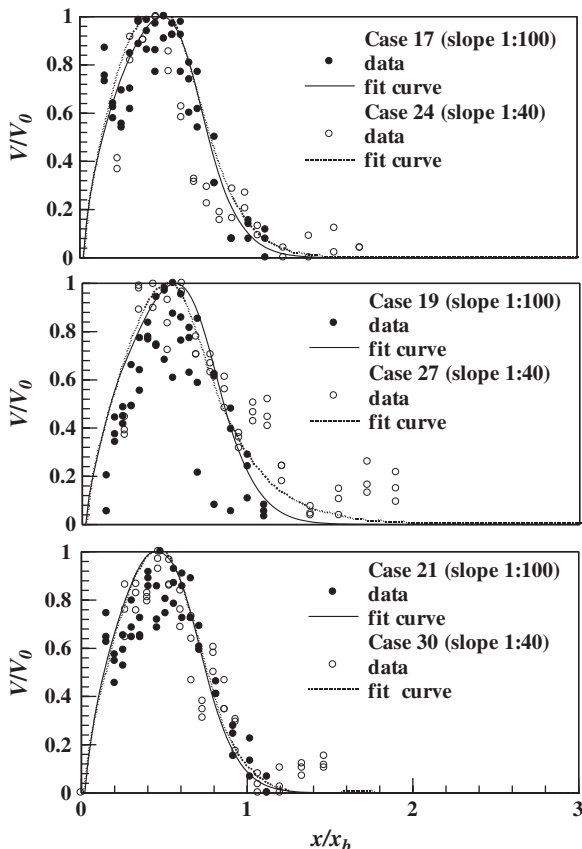


Fig. 20. Dimensionless velocity profiles for cases 17, 22, 19, 25, 21, and 28.

Table 6
Dimensionless results calculated from velocity profiles in Fig. 20.

Case	Slope	k'_0	c'_r	$T' = 2\pi/(k'_0 c'_r)$	T (s)
17	1:100	2.99	0.639	3.29	253.87
19	1:100	2.98	0.628	3.36	182.40
21	1:100	2.95	0.638	3.34	225.74
22	1:40	2.75	0.674	3.39	92.45
25	1:40	2.87	0.680	3.22	89.11
28	1:40	3.12	0.708	2.84	90.10

Note: k'_0 is the dimensionless wave number corresponding to the maximum growth rate; c'_r is the dimensionless propagation speed corresponding to k'_0 , $T = 2\pi[(k'_0/x_b)c'_r V_0]^{-1} = (T x_b)/V_0$.

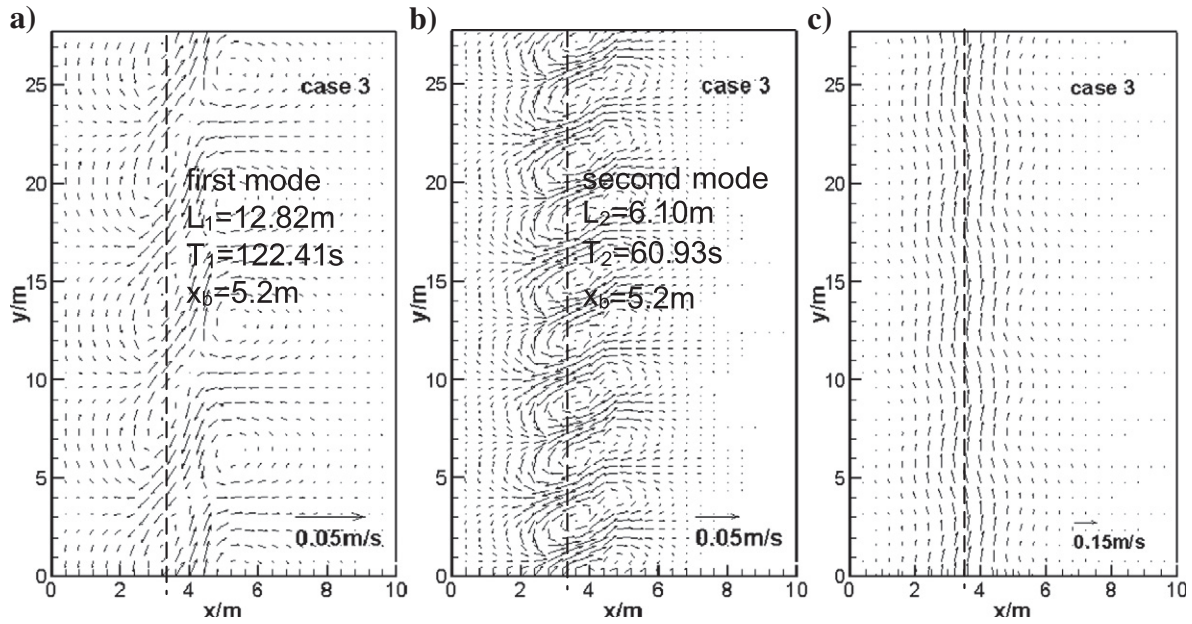


Fig. 21. (a) Calculated perturbation velocity fields according to the first mode (backshear mode) for case 3; (b) according to the second mode (frontshear mode) for case 3; (c) total velocity field superposed on mean longshore currents for case 3. The shear wave velocity has been scaled so that its peak magnitude equals one-sixth of the peak mean longshore current.

while V4 has the same frontshear as V1. The cross-shore gradients of these velocity profiles and the corresponding growth rate, ω_i' , and propagation speed, c_r' , are shown in Fig. 23(b), (c) and (d).

The wave number, k_0' , corresponding to the maximum growth rate, the propagation speed, c_r' , corresponding to k_0' , and the period of the shear waves ($T' = 2\pi(k_0'c_r')^{-1}$) for these velocity profiles are given in Table 7, along with the corresponding dimensional period $T = 2\pi[(k_0'/x_b)c_r'V_0]^{-1} = T'x_b/V_0$. For case 27, $x_b = 10.0$ m and $V_0 = 0.30$ m/s. Comparing V1 and V2, and noting that V1 has a frontshear extremum but V2 does not, we see that the frontshear extremum leads to a 15.92% $((3.64 - 3.14)/3.14 = 15.92\%)$ decrease in

k_0' and a 9.5% $((2.65 - 2.42)/2.42 = 9.5\%)$ increase in T' . The effect of the frontshear extremum on the backshear instability is similar to that discussed by Baquerizo et al. (2001), who analyzed data measured at Leadbetter Beach by increasing the shear at the front side of the longshore current and showed that the frontshear causes a 7.84% $((0.055 - 0.051)/0.051 = 7.84\%)$ decrease in the wave number for $c_d = 0.007$. The effect of varying the backshear can be seen in Table 7, where V3 shows a 105.61% $((2.420 - 1.177)/1.177 = 105.61\%)$ decrease in T' compared with V2. The large difference caused by variation in backshear and the small difference caused by variation in frontshear suggest that shear instability is sensitive to backshear but

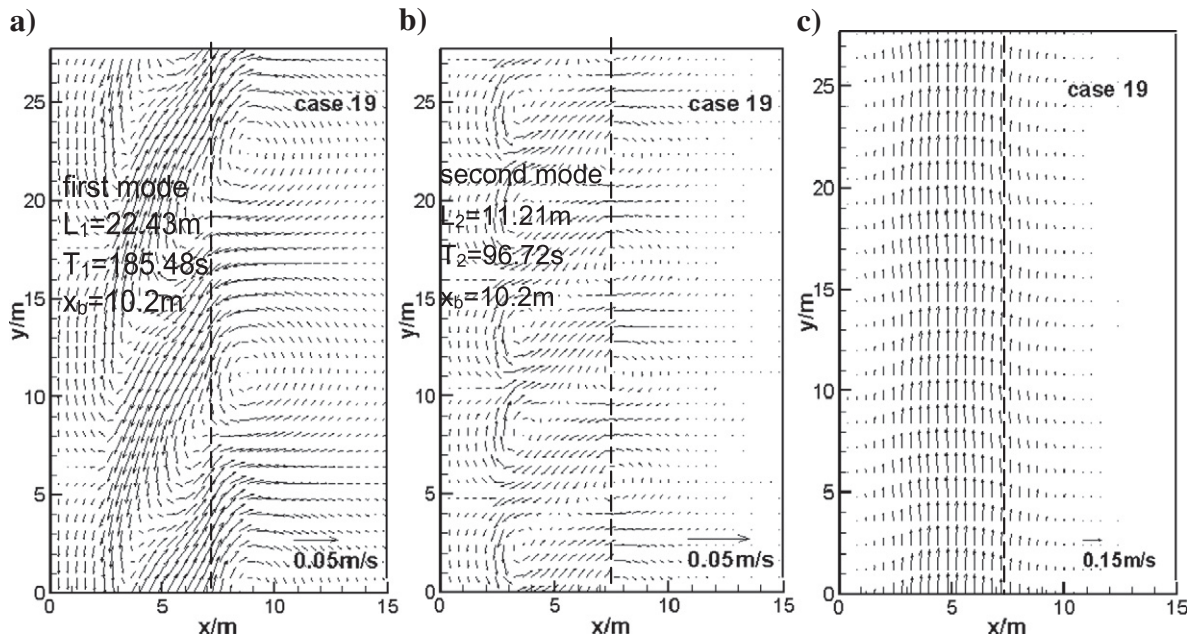


Fig. 22. (a) Calculated perturbation velocity fields according to the first mode (backshear mode) for case 19; (b) according to the second mode (frontshear mode) for case 19; (c) total velocity field superposed on mean longshore currents for case 19. The shear wave has been scaled so that its peak magnitude equals the one-sixth of the peak mean longshore current.

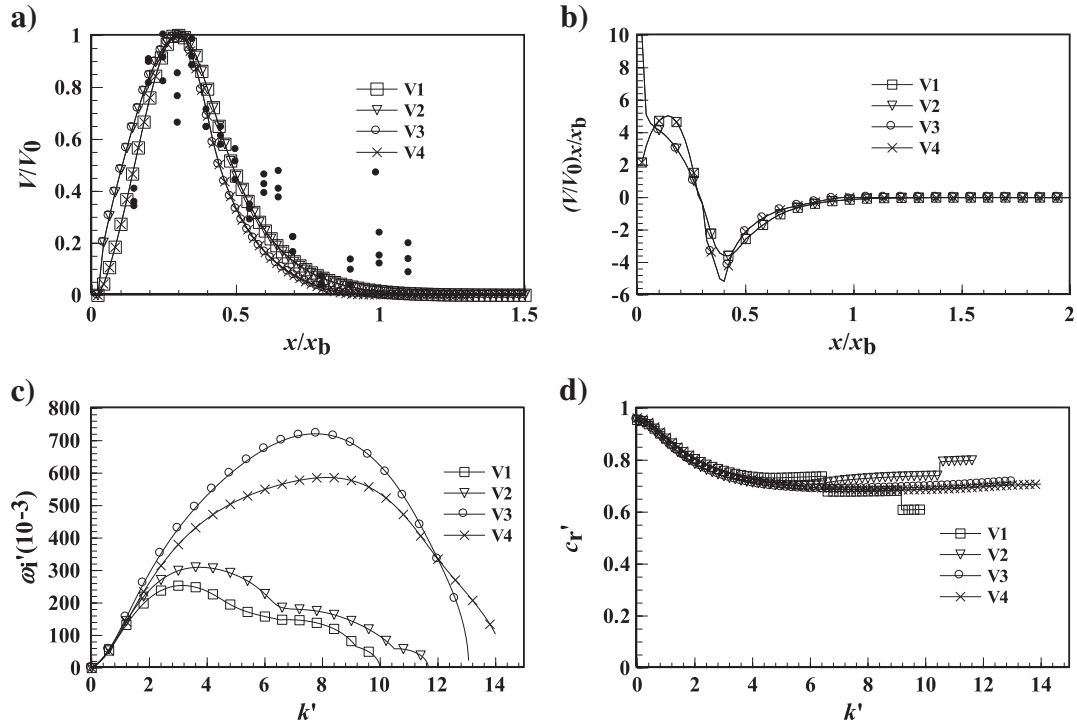


Fig. 23. (a) The four dimensionless current profiles for case 27; (b) dimensionless velocity gradients; (c) dimensionless growth rate; (d) dimensionless propagation speed.

not to frontshear. This demonstrates that backshear instability is the instability mode for case 27, where the inflection point is at the back side of the velocity profile (seaward side of the current).

Comparing V2 and V4, the latter having stronger frontshear and backshear than the former, allows the combined effect of variation in frontshear and backshear to be investigated. It is seen that V4 has a 114.92% $((2.420 - 1.126)/1.126 = 114.92\%)$ decrease in T' compared with V2.

The comparison of the dimensional periods of shear waves given by the four velocity profiles V1, V2, V3 and V4 with the corresponding experimental results in Table 4 shows that the periods for V1 and V2 are in agreement with experimental results, but differ considerably for V3 and V4.

The four velocity profiles chosen for case 21, V1', V2', V3' and V4', corresponding to V1, V2, V3 and V4 above, are given in Fig. 24. The differences between backshear and frontshear for each are the same as those for case 27. The calculated wave number, k'_0 , the propagation speed, c'_r , and the period of shear waves, T' , are given in Table 8, along with the corresponding dimensional period, $T = T'x_b/V_0$, for $x_b = 9.8$ m and $V_0 = 0.152$ m/s. The effects of the different four velocity profiles on the results are found to be similar to those for case 27. In Table 8, the change in T' are: 7.53% decrease from V1' to V2'; 53.61% increase from V2' to V3'; and 47.18% increase from V2' to V4'. The trends and magnitudes of the changes are similar to those for case 27. From these results, it is suggested that although the frontshear extremum causes only a 9.5% increase in T' for the 1:40 slope and 7.53% for the 1:100 slope, the change of backshear causes decreases of about 105.61% in T' for the 1:40 slope and 53.61% for the 1:100 slope. This demonstrates again that the instability mode is the cause of backshear instability.

6.4. Effects of regular and irregular waves

The present experimental results show that the periods of shear waves are about 50 s for regular waves and 100 s for irregular waves, for both the 1:100 and 1:40 slopes. The reason for this phenomenon is to do with the different surf zone widths for regular and irregular waves: that

is, narrower surf zone for regular waves and wider surf zone for irregular waves. In the figures, this is reflected in the velocity profiles, which are narrower for regular waves and wider for irregular waves.

7. Conclusions

A physical laboratory study of the instability of longshore currents was conducted for two plane beaches sloping at 1:100 and 1:40. A dye-dispersion experiment was also performed to investigate visually and spatially the shear instability of longshore currents.

Oscillations of the alongshore currents were observed for all test cases. Since the long-period oscillation was not indicated by dye patch movements outside the surf zone, the instability was not identified as being due to other kinds of motion such as wave basin seiching or other circulation caused by the limited size of the experiment arrangement.

The observed shear waves had dominant periods of approximately 100 s for irregular waves and a maximum amplitude of about one-sixth of the maximum mean alongshore currents. The propagation speeds of the shear waves were obtained by measuring the movement of the dye patch crest, and were found to be between one-half and three-quarters of the maximum mean alongshore currents.

Strong nonlinear shear instability was also observed in the alongshore currents. Their behavior was analyzed from the large deformations of dye

Table 7
Nondimensional results corresponding to V1–V4 for case 27.

Current profile	First mode				Second mode			
	k'_0	c'_r	$T' = 2\pi / (k'_0 c'_r)$	$T(s)$	k'_0	c'_r	$T' = 2\pi / (k'_0 c'_r)$	$T(s)$
V1	3.14	0.755	2.650	88.33	6.79	0.679	1.362	45.40
V2	3.64	0.712	2.420	80.67				
V3	7.75	0.689	1.177	39.23				
V4	8.14	0.685	1.126	37.53				

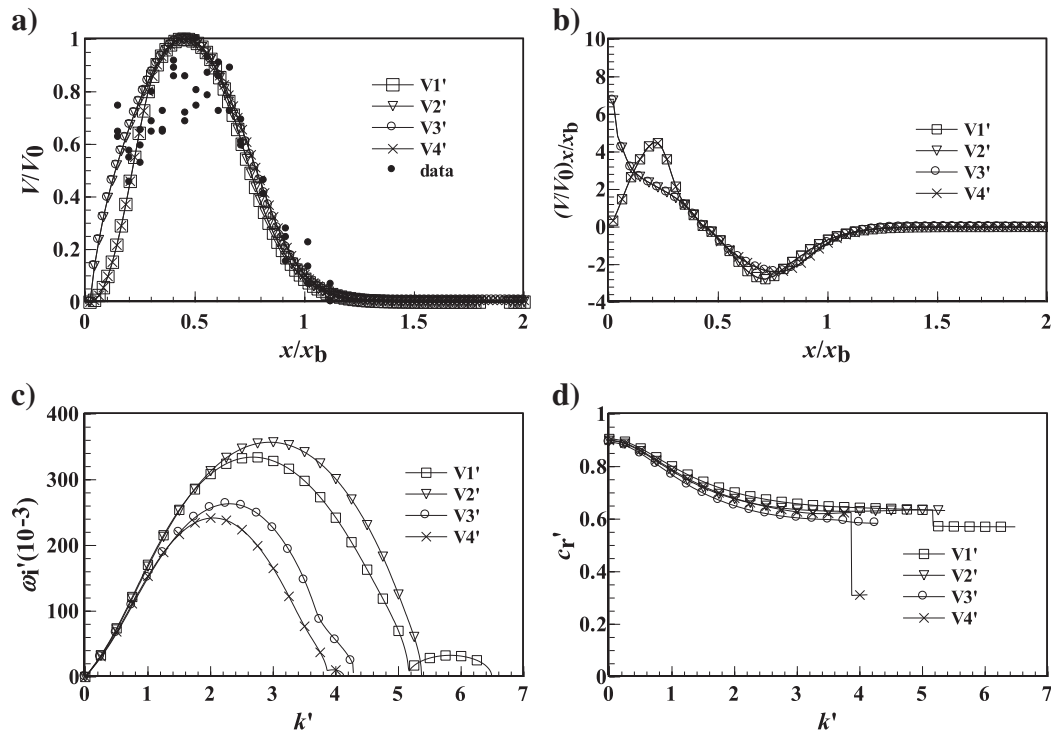


Fig. 24. (a) The four dimensionless current profiles for case 21; (b) dimensionless velocity gradients; (c) dimensionless growth rate; (d) dimensionless propagation speed.

Table 8

Nondimensional results corresponding to V1'–V4' for case 21.

Current profile	First mode				Second mode			
	k'_0	c'_r	$T' = 2\pi / (k'_0 c'_r)$	$T(s)$	k'_0	c'_r	$T' = 2\pi / (k'_0 c'_r)$	$T(s)$
V1'	2.67	0.669	3.516	226.69	5.82	0.572	1.886	121.60
V2'	2.95	0.638	3.337	215.15				
V3'	2.30	0.631	4.326	278.91				
V4'	2.04	0.676	4.554	293.61	3.96	0.311	5.100	328.82

patches and the presence of large-scale vorticity, the latter evidenced by vortex-shaped, multidirectional, complex dye movements.

Numerical analysis of the observed current profiles yielded shear instability periods of approximately 100 s for the 1:40 slope, in agreement with the experiment. However, disagreement occurred for the 1:100 slope: the calculated period of the shear waves was about 200 s whereas the corresponding observed period was about 100 s. The reason for this discrepancy was investigated from several aspects, including a theoretical analysis of different slope effects, the effect of changes in front- and backshear, and the effect of the frontshear mode. It was found that none of these explain the discrepancy. We did, however, confirm that different slopes will, in theory, generate a different shear wave period, and that the calculated result is theoretically sound, but an explanation of the discrepancy needs to be further investigated.

In the present study, linear instability analysis of the velocity profiles with and without an extremum of background vorticity at the front side of the mean longshore current peak showed that the frontshear mode contributes only a 9.5% increase in the period of dominant backshear instability, but the frontshear mode, if present, may be dominant. Its effect was examined by assuming an artificial extremum of background vorticity at the front side of the mean longshore current peak. The change of backshear may cause a decrease in the period of dominant backshear instability of the order of 105.61%.

Acknowledgement

The authors would like to thank the National Natural Science Foundation of China for financial support under Grant Nos. 50479053 and 10672034, and the support of the Program for Changjiang Scholars and Innovative Research Team at the University, and the support of the ShanXi Province Natural Science Foundation for Young Scholar (2011021025-1).

References

- Allen, J.S., Newberger, P.A., Holman, R.A., 1996. Nonlinear shear instabilities of alongshore currents on plane beaches. *J. Fluid Mech.* 310, 181–213.
- Baquerizo, A., Caballeria, M., Losada, M.A., Falques, A., 2001. Frontshear and backshear instabilities of the mean longshore current. *J. Geophys. Res.* 106 (C8), 16997–17011.
- Bowen, A.J., Holman, R.A., 1989. Shear instabilities of the mean longshore current, 1. Theory. *J. Geophys. Res.* 94 (C12), 18023–18030.
- Burg, J.P., 1967. Maximum entropy spectral analysis. 37th Ann. Int. Meet. Soc. Exploration Geophys., Oklahoma City.
- Dodd, N., Thornton, E.B., 1990. Growth and energetics of shear waves in the nearshore. *J. Geophys. Res.* 95, 16075–16083.
- Dodd, N., Oltman-shay, J., Thornton, E.B., 1992. Shear instabilities in the longshore current: a comparison of observations and theory. *J. Phys. Oceanogr.* 22, 62–82.
- Golub, G.H., Van Loan, C.F., 1996. *Matrix Computation*. The Johns Hopkins University Press, Baltimore.
- Householder, A.S., 1958. Unitary triangularization of a nonsymmetric matrix. *J. Assoc. Comput. Mach.* 5, 339–342.
- Kane, R.P., 1999. Prediction of the sunspot maximum of solar cycle 23 by extrapolation of spectral components. *Solar Physics* 189, 217–224.
- Kane, R.P., Trivedi, N.B., 1982. Comparison of maximum entropy spectral analysis (MESA) and least-squares linear prediction (LSLP) methods for some artificial samples. *Geophys* 47, 1731.
- Noyes, J.T., Guza, R.T., Elgar, S., Herbers, T.H.C., 2004. Field observations of shear waves in the surf zone. *J. Geophys. Res.* 109, C0103. doi:10.1029/2002JC001761.
- Oltman-Shay, J., Howd, P.A., Birkemeier, W.A., 1989. Shear instabilities of the mean longshore current, 2. Field observations. *J. Geophys. Res.* 94 (C12), 18031–18042.
- Özkan-Haller, H.T., Kirby, J.T., 1999. Nonlinear evolution of shear instabilities of the longshore current: a comparison of observations and computations. *J. Geophys. Res.* 104 (25), 953–25984.
- Putrevu, U., Svendsen, I.A., 1992. Shear instability of longshore currents: a numerical study. *J. Geophys. Res.* 97, 7283–7303.

- Reniers, A.J.H.M., Battjes, J.A., Falqués, A., Huntley, D.A., 1997. A laboratory study on the shear instability of longshore current. *J. Geophys. Res.* C4 (102), 8597–8609.
- Sancho, F.E.P. (1998), Unsteady nearshore currents on longshore varying topographies. Ph.D. thesis, University of Delaware, Dept. of Civil Engineering.
- Sawada, Y., Ohtomo, N., Tanaka, Y., 1997. New technique for time series analysis combining the maximum entropy method and non-linear least squares method: its value in heart rate variability analysis. *Med. Biol. Eng. Comput.* 35 (4), 318–322.
- Slinn, D.N., Allen, J.S., Newberger, P.A., Holman, R.A., 1998. Nonlinear shear instabilities of alongshore currents over barred beaches. *J. Geophys. Res.* 103 (C9), 18357–18380.
- Tiessen, M.C.H., van Leeuwen, S.M., Calvete, D., Dodd, N., 2010. A field test of a linear stability model for crescentic bars. *Coastal Eng.* 1, 41–51.
- Visser, P.J., 1982. Laboratory measurements of uniform longshore currents. *Coastal Eng.* 15, 563–593.